

# Optimum LoRaWAN Configuration Under Wi-SUN Interference

Arliones Hoeller, Richard Demo Souza, Hirley Alves, Onel L. Alcaraz López,  
Samuel Montejo-Sánchez, Marcelo Eduardo Pellenz

**Abstract**—Smart Utility Networks (SUN) rely on the Wireless-SUN (Wi-SUN) specification for years. Recently practitioners and researchers have considered Low-Power Wide-Area Networks (LPWAN) like LoRaWAN for SUN applications. With distinct technologies deployed in the same area and sharing unlicensed bands, one can expect these networks to interfere with one another. This paper builds over a LoRaWAN model to optimize network parameters while accounting for inter-technology interference. Our analytic model accounts for the interference LoRaWAN receives from IEEE 802.15.4G networks, which forms the bottom layers of Wi-SUN systems. We derive closed-form equations for the expected reliability of LoRaWAN in such scenarios. We set the model parameters with data from real measurements of the interplay among the technologies. Finally, we propose two optimization algorithms to determine the best LoRaWAN configurations, given a targeted minimum reliability level. The algorithms maximize either communication range or the number of users given constraints on the minimum number of users, minimum communication range, and minimum reliability. We validate the models and algorithms through numerical analysis and simulations. The proposed methods are useful tools for planning interference-limited networks with requirements of minimum reliability.

**Keywords**—Internet-of-Things, Low-Power Wide-Area Networks, Communication Interference.

## I. INTRODUCTION

Smart Utility Networks (SUN) are key enablers of Smart Cities [1]. In such environments, the Internet-of-Things (IoT) plays a paramount role in connecting massive numbers of

A. Hoeller and R.D. Souza are with the Department of Electrical and Electronics Engineering, Federal University of Santa Catarina, Florianópolis, 88040-900 Brazil.

A. Hoeller is also with the Department of Telecommunications Engineering, Federal Institute for Education, Science, and Technology of Santa Catarina, São José, 88103-310 Brazil.

A. Hoeller, H. Alves, and O.L.A. López are with Centre for Wireless Communications, University of Oulu, Oulu, 90014 Finland.

S. Montejo-Sánchez is with Programa Institucional de Fomento a la I+D+i, Universidad Tecnológica Metropolitana, Santiago, 8940577 Chile.

M.E. Pellenz is with the Informatics Graduate Program, Pontifical Catholic University of Paraná, Curitiba, 80215-901 Brazil.

Correspondence author: Arliones.Hoeller@ifsc.edu.br.

This work has been partially supported in Brazil by the National Council for Scientific and Technological Development (CNPq), Print CAPES-UFSC “Automation 4.0”, and INESC P&D Brasil (Project F-LOCO, Energisa, ANEEL PD-00405-1804/2018); in Finland by Academy of Finland (Aka) 6Genesis Flagship (Grant 318927), EE-IoT (Grant 319008) and Aka Prof (Grant 307492); and in Chile by FONDECYT Postdoctoral (Grant 3170021).

©2019 IEEE. Personal use of this material is permitted. Permission from IEEE must be obtained for all other uses, in any current or future media, including reprinting/republishing this material for advertising or promotional purposes, creating new collective works, for resale or redistribution to servers or lists, or reuse of any copyrighted component of this work in other works.

devices like smart meters, smart light bulbs, and smart appliances. Besides the existence of several potential network technologies, *e.g.*, LoRaWAN, SigFox, and Wi-SUN, the reliable and efficient connection of massive numbers of devices is still a challenge [2].

Industry backs two initiatives: LoRa Alliance and Wi-SUN Alliance. LoRa Alliance – supported by Semtech, IBM, Cisco, Orange, among others – maintains the LoRaWAN specification [3]. LoRaWAN is a Low-Power Wide-Area Network (LPWAN) technology operating in the sub-GHz ISM band, using chirp spread-spectrum modulation, allowing increased signal robustness and range at low power consumption and low data rates [1]. LoRaWAN uses the LoRa physical layer (PHY) designed by Semtech and specifies the upper layer protocols to enable IoT deployments. Wi-SUN Alliance – supported by Cisco, Analog Devices, Toshiba, and others – maintains the Wi-SUN specification [4], [5]. Wi-SUN is a Field Area Network (FAN) technology built upon the physical and link layers defined by the IEEE 802.15.4G standard. IEEE 802.15.4G operates in different ISM bands, including the same sub-GHz bands used by LoRaWAN, where it employs a Gaussian Frequency Shift Keying (GFSK) modulation over narrow-band channels. Wi-SUN also defines network- and application-level services and profiles for different utility applications (*e.g.*, energy, gas, water).

While utility service providers modernize their systems to use smart meters, deployments can use different communication technologies in the same geographical region, thus raising the question of how inter-technology interference affects network scalability. Coordination among transmissions in different technologies is unfeasible at the network or lower layers, so it is essential to understand the impact of external interference through use cases, theoretical analysis, and design strategies [6]. To achieve a realistic model, one should take into account that LPWAN devices in the ISM radio band are subject to interference generated by other networks sharing the same part of the spectrum. For instance, different authors report the analysis of the interaction of LoRa with other technologies considering IEEE 802.15.4G [7], SigFox [8], [9], and IEEE 802.11AH [9]. The results in those papers suggest that LoRa susceptibility to interference arriving from other technologies depends not only on the activity on those interfering networks but also on the configuration of the LoRa signal, mainly the spreading factor (SF). In this paper, we consider LoRaWAN as our target technology and model its performance in the presence of IEEE 802.15.4G interference sources in the sub-GHz ISM band (*e.g.*, around 868 MHz

in Europe and 915 MHz in USA/Brazil). Please note that the restriction of the model to IEEE 802.15.4G interference comes without loss of generality since one can extend it to other network technologies provided that appropriate isolation thresholds between the technologies are available.

In our work, we evolve from previous developments in [10] and [11] to approach the problem from an analytic perspective. We derive two optimization algorithms that explore the configuration space of LORAWAN in the presence of internal and external interference. The algorithms are network planning tools for massive IoT applications, guiding the trading-off between reliability, the number of users, and coverage area/range. We validate our analytic findings with simulations configured according to experimental results on the interplay of these networks published in [7]. We do not consider latency in this paper because our methods do not impact latency. A good third-party work that analyzes the latency of Class A LORAWAN is [12].

The contributions of this work include a closed-form expression for the inter-SF LORAWAN interference model of [11]; the extension of the analytic models of [10] and [11] to consider external interference; the performance analysis of LORAWAN considering the experimental results on inter-technology interference from [7]; and two algorithms to optimize LORAWAN configuration, either in terms of network load or communication range, under reliability constraints.

The remaining of this paper is organized as follows. Section II summarizes related work, and Section III briefly introduces the characteristics of LORAWAN and IEEE 802.15.4G. Section IV introduces the proposed models. Section V presents the proposed algorithms. Section VI evaluates the models and algorithms. Section VII concludes the paper.

## II. RELATED WORK

Georgiou and Raza [13] propose an analytic model of LORAWAN, which considers both disconnection and collision probabilities in Rayleigh fading channels. They show that LORAWAN is sensitive to node density because it affects collision probability. In [10], we extend the work of [13] to exploit message replications and multiple receive antennas at the gateway. We show that message replication is an interesting option for low-density networks, while the performance gains from spatial diversity are significant in all cases. Mahmood *et al.* [11], as well as we [10] and Georgiou and Raza [13], use stochastic geometry and Poisson Point Processes (PPP) to derive analytic models of the LORAWAN coverage probability. Contrasting with [13] and [10], the work in [11] considers the effect of interference from the imperfect orthogonality of LORA signals with different SF.

Orfanidis *et al.* [7] report an experimental evaluation of the interference between IEEE 802.15.4G and LORA by measuring the packet error ratio in different SINR scenarios inside an anechoic chamber. The measurements consider a single IEEE 802.15.4G interferer over one LORA link. Their results show that lower SFs are more susceptible to interference. Although these measurements show interesting results, it is important to note that they consider a limited number of nodes,

thus making it hard to extrapolate the conclusions. To the best of our knowledge, no other work has studied the susceptibility of LORA to external IEEE 802.15.4G interference, and there is none published work that investigates this relationship in a network-scale scenario with several active links in both IEEE 802.15.4G and LORAWAN.

## III. LPWAN NETWORKS

LPWAN technologies employ low-power communication mechanisms to enable the connection of thousands of IoT devices. Most technologies work in sub-GHz frequencies and feature link budgets of  $150 \pm 10$  dB, implementing robust communication channels with low energy consumption reaching distances in the order of kilometers [1]. For reducing complexity and energy consumption, LPWANs use MAC protocols that may decrease channel usage efficiency. For instance, the unslotted ALOHA MAC in LORAWAN presents high collision probability with large numbers of users [14].

### A. LORAWAN

LORA is a proprietary sub-GHz chirp spread spectrum modulation technique optimized for long-range low-power applications at low data rates [3]. LORA modulation depends, basically, on three parameters [15]: bandwidth ( $B$ ), usually set to 125 kHz or 250 kHz for uplink and 500 kHz for downlink; SF, which assumes values from 7 up to 12; and the forward error correction (FEC) rate, varying from  $\frac{4}{8}$  to  $\frac{4}{5}$ . The parameters allow computing packet Time-on-Air (ToA), receiver sensitivity, and required signal-to-noise ratio (SNR) for successful detection in the absence of interference, which Table I presents for a given packet configuration. Note that ToA grows exponentially with SF, reducing the data rate and decreasing receiver sensitivity, improving coverage.

Table I  
LORA UPLINK CHARACTERISTICS FOR 9-BYTE PACKETS,  $B = 125$  KHZ, CRC AND HEADER MODE ENABLED, AND FEC RATE  $\frac{4}{5}$  FOR THE SX1272 TRANSCEIVER [16].

SF $i$	ToA $t_i$ (ms)	Bitrate $Rb_i$ (kbps)	Receiver Sensitivity $S_i$ (dBm)	SNR threshold $\psi_i$ (dB)
7	41.22	5.47	-123	-6
8	72.19	3.12	-126	-9
9	144.38	1.76	-129	-12
10	247.81	0.98	-132	-15
11	495.62	0.54	-134.5	-17.5
12	991.23	0.29	-137	-20

The LORA PHY is agnostic of higher layers. LORAWAN is the most widely used protocol stack for LORA networks. It implements a star topology where *end-devices* (nodes) connect through a single-hop to one or more *gateways*, which in turn connect to a *network server* via an IP network. Moreover, a LORA gateway can process up to nine channels in parallel, combining different sub-bands and SF [1]. LORA features the capture effect, making it possible to recover a LORA signal when two or more signals are received simultaneously, in the same frequency and SF, provided that the desired signal is at least 1 dB above interference [17].

## B. IEEE 802.15.4G

IEEE 802.15.4G is an amendment to the IEEE 802.15.4 standard focusing on Smart Utility Networks (SUN) that plays an important role in the smart grid [18]. The standard specifies several modes operating in different bands, including the Sub-GHz ISM bands used by LORAWAN. Multi-Rate FSK (MR-FSK), with 2-FSK or 4-FSK, is the predominant modulation version in SUN applications due to its communication range [19]. In this configuration, the transceiver combines FSK modulation with Frequency Hopping Spread Spectrum (FHSS) to increase robustness [20]. Data rate varies from 2.4 to 200 kbps, depending on region and frequency band.

The mandatory configuration for all regions is 2-FSK operating at 50 kbps, which implies a channel spacing of 200 kHz. Transmit power depends on regional regulations, but must be at least  $-3\text{dBm}$  [5]. Most configurations use 14dBm transmit power and 1% duty cycle [21]. IEEE 802.15.4G also extends the MAC mechanisms defined by IEEE 802.15.4E amendment [22] to make extensive use of low-energy modes. IEEE 802.15.4G networks are expected to form multi-hop, mesh networks. Before sending data, the MAC performs either carrier sense or a simplified version of channel monitoring named Coordinated Sampled Listening (CSL) [23].

## IV. SYSTEM MODEL

Following the developments in [10] and [11], we use a set of Poisson Point Processes (PPP) [24]. Our model considers nodes deployed uniformly in a circular region around a gateway. Figure 1 illustrates a *possible* setup where SF increases according to the distance from the gateway. The figure, as in previous related work, uses fixed-width SF rings which are sub-optimal, an issue that is addressed by us in Section V. The vector  $L = [l_0, \dots, l_6]$ ,  $l_0 = 0$ , defines the limits of each SF ring. Note that  $R = l_6$  is the maximum network communication range, *i.e.*, the coverage radius. LORAWAN devices transmit in the uplink at random using the ALOHA protocol and transmit once in a given period  $T$ . Considering that all nodes run the same application, the network usage is different for each SF because of different data rates (see ToA in Table I). Figure 1 also shows the ToA difference graphically. Hence, we model the transmission probability of LORAWAN devices as a vector  $p = [p_1, \dots, p_6]$ ,  $p_i \in (0, 1] \forall i \in \{1, \dots, 6\}$ , and  $p_i = \frac{t_i}{T}$ , where  $t_i$  is the ToA for SF of ring  $i$ . Note that, for the sake of simplicity, we define the set  $S = \{1, \dots, 6\}$  to denote the SF rings and that each ring uses a respective SF in  $\{7, \dots, 12\}$ .

Each LORAWAN SF ring constitutes a separated PPP, denoted  $\Phi_i, i \in S$ , making it possible to attribute different densities to each SF.  $\Phi_i$  has density  $\alpha_i = p_i \rho_i$  in its area  $V_i = \pi(l_i^2 - l_{i-1}^2)$ , where  $l_{i-1}$  and  $l_i$  are, respectively, the inner and outer radii of SF ring  $i$  (from  $L$ ), and  $\rho_i$  is the spatial density of nodes in  $V_i$ . The average number of nodes in  $\Phi_i$  is  $\bar{N}_i = \rho_i V_i$ . The average number of nodes in the LORAWAN network is  $\bar{N} = \sum_{i \in S} \rho_i V_i$ . For instance, take the ring  $i = 2$  in Figure 1, defined by two circles of radii  $l_1 = 2\text{km}$  and  $l_2 = 4\text{km}$ . Nodes in this ring use SF<sub>8</sub>. The ring area is  $V_2 = \pi(l_2^2 - l_1^2) = 37.7\text{km}^2$ . If there are, on

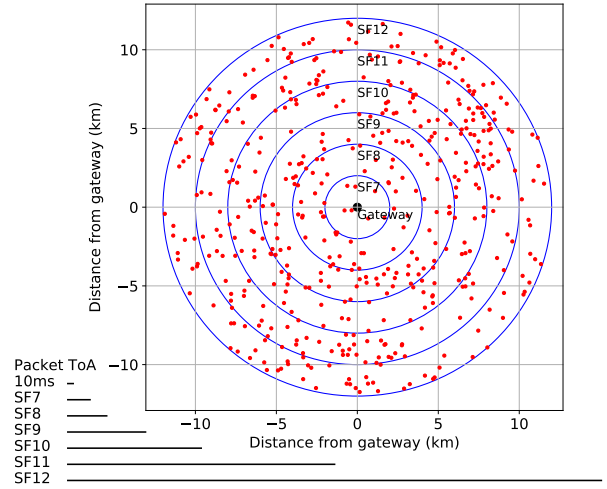


Figure 1.  $\bar{N} = 500$  nodes uniformly distributed in a circular area of radius  $R = 12000$  m around the gateway and with increasing SF every 2000 m. The ToA, as in Table I, is illustrated in the lower-left corner.

average,  $\bar{N}_2 = V_2 \rho_2 = 100$  nodes in this ring, then its spatial density is  $\rho_2 = \frac{\bar{N}_2}{V_2} = 2.65$  nodes/ $\text{km}^2$ . Finally, if nodes transmit probability is 1% ( $p_2 = 0.01$ ), the intensity of  $\Phi_2$  is  $\alpha_2 = p_2 \rho_2 = 0.0265$ .

In addition to LORAWAN, we consider an external IEEE 802.15.4G network operating in the same ISM bands and geographic region. Users of that network are spread across the LORAWAN area. IEEE 802.15.4G transceivers in ISM sub-GHz bands employ bandwidth and transmit power configurations similar to LORAWAN. So, we model the IEEE 802.15.4G network as an additional PPP where nodes transmit with probability  $p_z \in (0, 1]$  in area  $V_z = \pi R_z^2$ , where  $R_z \geq R$ . The PPP  $\Phi_z$  has density  $\alpha_z = p_z \rho_z$ , where  $\rho_z$  is the spatial density of nodes in  $V_z$ . The average number of nodes in  $\Phi_z$  is  $\bar{N}_z = \rho_z V_z$ .

In our analysis,  $d_k$  is the Euclidean distance between the  $k$ -th node and the gateway, and  $d_1$  denotes the distance of the node of interest. All nodes use the same transmit power  $\mathcal{P}_t$  to send signal  $s_k$ , while both path loss and Rayleigh fading affect the received signals of LORAWAN and IEEE 802.15.4G. Path loss follows  $g(d_k) = \left(\frac{\lambda}{4\pi d_k}\right)^\eta$ , with wavelength  $\lambda$ , path loss exponent  $\eta \geq 2$ , while  $k$  represents a device in either network. Finally,  $h_k$  denotes the Rayleigh fading. Therefore, a LORAWAN signal  $r_1$  received at the gateway is the sum of the attenuated transmitted signal  $s_1$ , interference, and noise,

$$r_1 = g(d_1)h_1 s_1 + \mathcal{I}_L + \mathcal{I}_Z + n, \quad (1)$$

where

$$\mathcal{I}_L = \sum_{i \in S} \sum_{k \in \Phi_i} g(d_k)h_k s_k \quad (2)$$

accounts for intra-network interference, considering both co-SF and inter-SF interference by summing all other received signals from all SFs, and

$$\mathcal{I}_Z = \sum_{k \in \Phi_z} g(d_k)h_k s_k \quad (3)$$

models external interference arising, in our case, from all active nodes in the IEEE 802.15.4G network. Finally,  $n$  is the additive white Gaussian noise (AWGN) with zero mean and variance  $\mathcal{N} = -174 + F + 10\log_{10}(B)$  dBm, where  $F = 6$  dB is the receiver noise figure and  $B = 125$  kHz is the LORA channel bandwidth. The remainder of this section uses this model to derive a reliability model of LORAWAN.

### A. Coverage Probability

The *coverage probability* is the probability that the selected node is in coverage (not in outage), *i.e.*, it can successfully communicate in the presence of noise, internal interference, and external interference. The coverage probability of the desired node located  $d_1$  meters from the gateway is thus

$$C_1(d_1) = H_1(d_1)Q_1(d_1)Z_1(d_1), \quad (4)$$

where  $H_1$ ,  $Q_1$ , and  $Z_1$  are described in the following sections and denote the success probability with regards to, respectively, noise, internal interference, and external interference.

### B. Outage Condition 1: Disconnection

Following [10], we consider the disconnection probability, which depends on the communication distance. A node is *not* connected to the gateway if the SNR of the received signal is below the threshold that allows successful detection in the absence of interference. Receiver sensitivity is different for each SF, what results in different SNR reception thresholds defined in

$$\Psi_{[dB]} = \begin{matrix} SF_7 & SF_8 & SF_9 & SF_{10} & SF_{11} & SF_{12} \\ [-6 & -9 & -12 & -15 & -17.5 & -20 ], \end{matrix}$$

where  $\Psi$  is the SNR threshold vector, and  $\psi_i$  denotes the  $i$ -th element of  $\Psi$ , *i.e.*, the SNR threshold for SF ring  $i$ . Then, we model the *connection probability* as

$$H_1(d_1) = \mathbb{P}[\text{SNR} \geq \psi_i | d_1]. \quad (5)$$

Since we assume Rayleigh fading, the instantaneous SNR is exponentially distributed [25], and therefore

$$H_1(d_1) = \mathbb{P} \left[ \frac{\mathcal{P}_t |h_1|^2 g(d_1)}{\mathcal{N}} \geq \psi_i \right] = \exp \left( - \frac{\mathcal{N} \psi_i}{\mathcal{P}_t g(d_1)} \right). \quad (6)$$

### C. Outage Condition 2: Intra-Network Interference

Intra-network interference arises from the activity of other devices in the same network. We follow [11] to model both co-SF and inter-SF interference. To recover a packet, the signal-to-interference ratio (SIR) at the gateway must be above a given threshold. The transceiver manufacturer informs that SFs are orthogonal and that the co-SF SIR threshold is +6dB [16]. Goursaud *et al.* [26] propose theoretical SIR thresholds that match Semtech co-SF value but show that different SFs are not entirely orthogonal. However, Croce *et al.* [17] showed, experimentally, that the SIR thresholds for Semtech SX1272 LORA transceiver are lower with regards to co-SF interference

( $\approx +1$  dB) but significantly higher with respect to (w.r.t.) inter-SF interference. In this paper, we assume the experimental SIR thresholds of [17]

$$\Delta_{[dB]} = \begin{matrix} SF_7 & SF_8 & SF_9 & SF_{10} & SF_{11} & SF_{12} \\ SF_7 & \begin{bmatrix} +1 & -8 & -9 & -9 & -9 & -9 \end{bmatrix} \\ SF_8 & \begin{bmatrix} -11 & +1 & -11 & -12 & -13 & -13 \end{bmatrix} \\ SF_9 & \begin{bmatrix} -15 & -13 & +1 & -13 & -14 & -15 \end{bmatrix} \\ SF_{10} & \begin{bmatrix} -19 & -18 & -17 & +1 & -17 & -18 \end{bmatrix} \\ SF_{11} & \begin{bmatrix} -22 & -22 & -21 & -20 & +1 & -20 \end{bmatrix} \\ SF_{12} & \begin{bmatrix} -25 & -25 & -25 & -24 & -23 & +1 \end{bmatrix} \end{matrix},$$

where  $\Delta$  is the SIR threshold matrix, and  $\delta_{i,j}$  denotes the element of  $\Delta$  at the  $i$ -th line and  $j$ -th column, *i.e.*, the SIR threshold for the desired signal using  $SF_i$  and interference using  $SF_j$ . Note that  $i = j$  relates to the co-SF SIR while  $i \neq j$  relates to inter-SF SIR. If one takes the  $SF_7$  column as an example, it shows how  $SF_7$  interference affects the LORA signals. Desired signals using higher SF are more robust to inter-SF interference, allowing for the decoding of LORA packets even if the interference power is much higher than the signal (*e.g.*, 25dB higher if the signal uses  $SF_{12}$ ).

Following this rationale, we first use the formulations in [11] to analyze the success probability considering the interference from only one different  $SF_j$ . Let

$$\text{SIR}_j = \frac{|h_1|^2 g(d_1) \mathcal{P}_t}{\mathcal{I}_j}, \quad (7)$$

where the interference received from nodes using  $SF_j$  is

$$\mathcal{I}_j = \sum_{k \in \Phi_j} |h_k|^2 g(d_k) \mathcal{P}_t. \quad (8)$$

Since the desired node at  $d_1$  uses  $SF_i$ , the success probability is

$$\begin{aligned} P_{\text{SIR}_j}(d_1, j) &= \mathbb{P}[\text{SIR}_j \geq \delta_{i,j}] \\ &= \mathbb{E}_{\mathcal{I}_j} \left[ \mathbb{P} \left[ |h_1|^2 \geq \frac{\mathcal{I}_j \delta_{i,j}}{g(d_1) \mathcal{P}_t} \right] \right]. \end{aligned}$$

Since  $|h_1|^2 \sim \exp(1)$ ,

$$P_{\text{SIR}_j}(d_1, j) = \mathbb{E}_{\mathcal{I}_j} \left[ \exp \left( - \frac{\mathcal{I}_j \delta_{i,j}}{g(d_1) \mathcal{P}_t} \right) \right]. \quad (9)$$

Note that (9) has the form of the Laplace Transform w.r.t.  $\mathcal{I}_j$ , where  $\mathcal{L}_{\mathcal{I}_j}(s) = \mathbb{E}_{\mathcal{I}_j}[\exp(-s\mathcal{I}_j)]$ ,  $s = \frac{\delta_{i,j}}{g(d_1)\mathcal{P}_t}$ . Thus, using (8) and applying the property of the sum of exponents,

$$P_{\text{SIR}_j}(d_1, j) = \mathbb{E}_{\Phi_j, |h_k|^2} \left[ \prod_{k \in \Phi_j} \exp(-s |h_k|^2 g(d_k) \mathcal{P}_t) \right].$$

Solving the expectation over  $|h_k|^2 \sim \exp(1)$  yields

$$P_{\text{SIR}_j}(d_1, j) = \mathbb{E}_{\Phi_j} \left[ \prod_{k \in \Phi_j} \frac{1}{1 + s g(d_k) \mathcal{P}_t} \right].$$

We solve the expectation over the PPP  $\Phi_j$  using the probability generating functional of the product over PPPs where  $\mathbb{E}[\prod_{x \in \Phi_j} f(x)] = \exp[-\alpha_j \int_{\mathbb{R}^2} (1 - f(x)) dx]$ , with  $\alpha_j$  as

the density of  $\Phi_j$ , converting  $d_k$  to polar coordinates, and replacing  $s$ , obtaining

$$P_{\text{SIR}_j}(d_1, j) = \exp\left(-2\pi\alpha_j \int_{l_{j-1}}^{l_j} \frac{\delta_{i,j} d_1^\eta}{x^\eta + \delta_{i,j} d_1^\eta} x \, dx\right). \quad (10)$$

As a contribution over [11], we provide in Appendix VII a closed-form solution for the integral in (10), which we isolate in function  $f(\cdot)$ . The solution is

$$f(d_1, \delta_{i,j}, l_{j-1}, l_j) = \frac{l_j^2}{2} {}_2F_1\left(1, \frac{2}{\eta}; 1 + \frac{2}{\eta}; -\frac{l_j^\eta}{d_1^\eta \delta_{i,j}}\right) - \frac{l_{j-1}^2}{2} {}_2F_1\left(1, \frac{2}{\eta}; 1 + \frac{2}{\eta}; -\frac{l_{j-1}^\eta}{d_1^\eta \delta_{i,j}}\right), \quad (11)$$

and therefore,

$$P_{\text{SIR}_j}(d_1, j) = \exp[-2\pi\alpha_j f(d_1, \delta_{i,j}, l_{j-1}, l_j)]. \quad (12)$$

Now we consider interference from all SFs when

$$\text{SIR} = \frac{|h_1|^2 g(d_1) \mathcal{P}_t}{\sum_{j \in \mathcal{S}} \mathcal{I}_j}. \quad (13)$$

Following [11], we consider that an outage takes place if the SIR for at least one interfering SF exceeds the threshold in  $\Delta$ . Conversely, the probability that a collision does not occur is

$$Q_1(d_1) = \prod_{j \in \mathcal{S}} P_{\text{SIR}_j}(d_1, j).$$

Since  $P_{\text{SIR}_j}$ , shown in (12), is an exponential function, we compute the above product by summing the exponents and reorganizing, obtaining

$$Q_1(d_1) = \exp\left(-2\pi \sum_{j \in \mathcal{S}} \alpha_j f(d_1, \delta_{i,j}, l_{j-1}, l_j)\right). \quad (14)$$

#### D. Outage Condition 3: External Interference

Orfanidis *et al.* [7] report the selectivity of LORA receivers in the presence of IEEE 802.15.4G signals. We use Orfanidis *et al.* experimentally obtained isolation thresholds to analyze the SIR in the presence of external interference generated by an IEEE 802.15.4G network. Here, we model the IEEE 802.15.4G network as PPP  $\Phi_z$  and consider [7]

$$\Theta_{[dB]} = \begin{bmatrix} SF_7 & SF_8 & SF_9 & SF_{10} & SF_{11} & SF_{12} \\ -6 & -9 & -12.5 & -16 & -16 & -16 \end{bmatrix},$$

where  $\Theta$  denotes the LORA vs. IEEE 802.15.4G SIR threshold vector, and  $\theta_i$  denotes the  $i$ -th element of  $\Theta$ , *i.e.*, the SIR threshold for the desired signal in SF ring  $i$  and interference from the IEEE 802.15.4G network.

The analysis of the LoRa capture probability in the presence of IEEE 802.15.4G interference is similar to the case for one SF ( $P_{\text{SIR}_j}$ ), but taking the  $\Theta$  vector and the IEEE 802.15.4G network parameters into account. For

$$\text{SIR}_z = \frac{|h_1|^2 g(d_1) \mathcal{P}_t}{\sum_{k \in \Phi_z} |h_k|^2 g(d_k) \mathcal{P}_t}, \quad (15)$$

the *capture probability* w.r.t. external interference is

$$Z_1(d_1) = P_{\text{SIR}_z}(d_1) = \exp(-2\pi\alpha_z f(d_1, \theta_i, 0, R_z)). \quad (16)$$

Note that the model for external interference supports any other communication technology given that adequate SIR thresholds of  $\theta$  are provided.

## V. OPTIMUM LORAWAN CONFIGURATION

The expressions in Section IV determine the expected reliability of a single node located at a given distance from the gateway. *However, what if one wants to plan the network deployment?* In this section, we consider the use of the previous model to this end. We first consider the inversion of the expressions in the model to obtain network configurations for a targeted minimum average reliability. Afterward, we propose two algorithms that derive optimum network configurations supporting the desired minimum reliability requirement.

### A. Guaranteeing the Reliability Target

To start our search for optimal LORAWAN configurations we invert the previously described outage expressions defined in (6) and (14), so the network parameters can be extracted from them to achieve a minimum desired reliability level. Note that (16) does not depend on the LORAWAN configuration. It is, however, taken into account in the optimization algorithm proposed in Sections V-B and V-C to consider external interference. One can assume that, in our network model, the nodes presenting the worst average reliability in each SF ring are those on the outer ring limit. It happens because the signals emitted by those nodes suffer greater path-loss and are, therefore, more susceptible to interference.

1) *SF Ring Limits:* As a first step, we find the maximum distance that ensures the required minimum average reliability level w.r.t. the connection probability  $H_1$ . We denote this threshold by  $\mathcal{T}_{H_1}$ . We rewrite (6) to perform operations over the SNR threshold  $\psi_i$  in  $\Psi$  and the outer SF ring limit  $l_i$ ,

$$\mathcal{T}_{H_1} = \exp\left(-\frac{\mathcal{N}\psi_i}{\mathcal{P}_t g(l_i)}\right), \quad (17)$$

and then it is straightforward to obtain

$$l_i = \frac{\lambda}{4\pi} \left[-\frac{\mathcal{P}_t \ln(\mathcal{T}_{H_1})}{\mathcal{N}\psi_i}\right]^{\frac{1}{\eta}}. \quad (18)$$

Note that the radius of the overall coverage area is  $R = l_6$ .

2) *Ring Densities:* Since (18) defines the network geometry, it is now possible to obtain the outage due to external interference observed by the nodes at each ring edge from  $Z_1(l_i)$ . After that, we compute the maximum densities of the PPPs in  $Q_1$  that satisfy the given final reliability target  $\mathcal{T}$ , the previously assumed connection reliability target  $\mathcal{T}_{H_1}$ , and the external interference of each SF  $i$ . Thus, following (4), making  $C_1(l_i) = \mathcal{T}$  and  $H_1(l_i) = \mathcal{T}_{H_1}$ , we have for each SF ring  $i$  that  $\mathcal{T} = \mathcal{T}_{H_1} Q_1(l_i) Z_1(l_i)$ , and thus

$$\frac{\mathcal{T}}{\mathcal{T}_{H_1} Z_1(l_i)} = \exp\left(-2\pi \sum_{j \in \mathcal{S}} \alpha_j f(l_i, \delta_{i,j}, l_{j-1}, l_j)\right). \quad (19)$$

In (19), the function  $f(\cdot)$  is independent of  $\alpha_j$  if the SF limits are pre-defined. Then, let  $y_{i,j} = f(l_i, \delta_{i,j}, l_{j-1}, l_j)$  and  $b_i = -\frac{1}{2\pi} \ln\left(\frac{\mathcal{T}}{\mathcal{T}_{H_1} Z_1(l_i)}\right)$ , yielding, for each SF ring  $i$ ,

$$y_{i,1}\alpha_1 + y_{i,2}\alpha_2 + y_{i,3}\alpha_3 + y_{i,4}\alpha_4 + y_{i,5}\alpha_5 + y_{i,6}\alpha_6 = b_i. \quad (20)$$

If we name the vectors  $A = [\alpha_1, \dots, \alpha_6]$ ,  $B = [b_1, \dots, b_6]$ , and matrix  $Y = [y_{i,j}], \forall i, j \in S$ , from (20), we derive a system of linear equations  $Y \times A = B$  and solve it for the PPP densities  $A$  by making

$$A = Y^{-1} \times B. \quad (21)$$

Note that  $Y$  is a  $|S| \times |S|$  square matrix, both  $A$  and  $B$  are row vectors of length  $|S|$ , and all values  $y_{i,j}$  in  $Y$  are positive real numbers. To be invertible ( $Y^{-1}$ ),  $Y$  must have a non-zero determinant. Considering the diagonal method to compute the determinant of  $Y$ , we observe that, due to  $\Delta$ , the values at  $i = j$  are significantly higher than when  $i \neq j$ , thus making the positive diagonal greater than the negative diagonal, yielding a determinant that is virtually never zero.

### B. Maximization of Communication Range

The expressions presented above allow us to obtain twelve network parameters: six communication range limits  $L = [l_1, \dots, l_6]$  from (18), and six PPP densities  $A = [\alpha_1, \dots, \alpha_6]$  from (21). Note that (21) depends on (18) because of  $L$ . Combining both equations generates an incomplete linear system of six equations and twelve variables. In order to search for optimized feasible network configurations, we propose an algorithm that uses (18) and (21) in an iterative method, trying to extend the outer SF ring limits as much as possible, while preserving the targeted final reliability level  $\mathcal{T}$  and ensuring service to a minimum quantity of nodes ( $N_{min}$ ). The algorithm extends the outer SF ring limits by reducing  $\mathcal{T}_{H_1}$ . Similarly, increasing  $\mathcal{T}_{H_1}$  shortens these limits. The algorithm iteratively guesses values for  $\mathcal{T}_{H_1}$  and then, after obtaining  $L$  through (18), analyzes the maximum possible densities  $A$ . As  $\mathcal{T}_{H_1}$  gets closer to  $\mathcal{T}$ , the capture probability  $Q_1$  increases and, with fixed  $L$  and  $Z_1$ , higher  $Q_1$  is possible only with lower densities. It may lead to configurations breaking the  $N_{min}$  restriction. Conversely, if  $\mathcal{T}_{H_1}$  is too close to 1, the outer limits of the SF rings will be shorter, leading to small coverage areas that are useless in practice. However, the proposed algorithm identifies feasible ranges for the network parameters, thus dealing with this parameter trade-off.

Algorithm 1 employs a bisection technique [27] to explore the network design space (*i.e.*, possible values of  $\mathcal{T}_{H_1}$ ), seeking to maximize the width of each SF ring and, as a consequence, the network communication range (disk radius), while preserving the targeted minimum reliability  $\mathcal{T}$  and ensuring service to, at least, a given number of nodes ( $N_{min}$ ). The bisection technique fits well to our problem because it accelerates convergence by reducing the design space in half in each iteration, and it is guaranteed to converge if the problem is feasible. The inputs of the algorithm are the targeted reliability  $\mathcal{T}$ , the duty-cycle vector  $p$ ,  $N_{min}$ , and the density of IEEE 802.15.4G interfering nodes  $\alpha_z$ . The algorithm outputs a *result* variable

stating if the algorithm converged (1) or not ( $-1$ ), the achieved number of nodes  $N$ , and the vectors  $L$  and  $A$  containing, respectively, the rings limits and densities ensuring the target reliability.

---

**Algorithm 1** Maximization of SF rings widths given the target reliability ( $\mathcal{T}$ ) and the minimum number of nodes ( $N_{min}$ ).

---

**Input:**  $\mathcal{T}, p, N_{min}, \alpha_z$

**Output:** result,  $A, L, N$

---

```

1:  $\mathcal{T}_{H_1, max} \leftarrow 1$ 
2:  $\mathcal{T}_{H_1, min} \leftarrow \mathcal{T}$ 
3:  $R \leftarrow 0, N \leftarrow 0$ 
4: result  $\leftarrow 0$ 
5: while result = 0 do
6:    $\mathcal{T}_{H_1} \leftarrow (\mathcal{T}_{H_1, max} + \mathcal{T}_{H_1, min})/2$ 
7:    $L \leftarrow \frac{\lambda}{4\pi} \left[ -\frac{\mathcal{P}_t \ln(\mathcal{T}_{H_1})}{N\psi} \right]^{\frac{1}{\eta}}$  {Equation (18)}
8:    $R_{last} \leftarrow R$ 
9:    $R \leftarrow L[end]$ 
10:   $R_z \leftarrow R$ 
11:  for  $i = [1, \dots, 6]$  do
12:    for  $j = [1, \dots, 6]$  do
13:       $Y[i, j] \leftarrow f(l_i, \delta_{i,j}, l_j, l_{j+1})$ 
14:    end for
15:     $B[i] \leftarrow -\frac{1}{2\pi} \ln \frac{\mathcal{T}}{Z_1(l_i)\mathcal{T}_{H_1}}$ 
16:  end for
17:   $A \leftarrow Y^{-1} \times B$  {Equation (21)}
18:   $V \leftarrow \text{ComputeRingAreas}(L)$ 
19:   $N \leftarrow (Ap) \times V'$ 
20:  if  $\text{abs}(R - R_{last}) < \chi$  and  $A_i \geq 0, \forall A_i$  then
21:    if  $N < N_{min}$  then
22:      if  $\mathcal{T}_{H_1, max} - \mathcal{T}_{H_1, min} < \epsilon$  then
23:        result  $\leftarrow -1$ 
24:      end if
25:    else
26:      result  $\leftarrow 1$ 
27:    end if
28:  end if
29:  if result = 0 then
30:    if  $A_i \geq 0, \forall A_i$  and  $N \geq N_{min}$  then
31:       $\mathcal{T}_{H_1, max} = \mathcal{T}_{H_1}$ 
32:    else
33:       $\mathcal{T}_{H_1, min} = \mathcal{T}_{H_1}$ 
34:    end if
35:  end if
36: end while
37: return result,  $A, L, N$ 

```

---

After initializing the variables (lines 1-4), the optimization loop starts and runs until the algorithm converges (line 26) or diverges (line 23). The optimization procedure “guesses” values for  $\mathcal{T}_{H_1}$ , trying to reduce it to enlarge the width of each SF ring, thus increasing the coverage area. Note that since  $C_1$  depends on  $H_1$  from (4),  $\mathcal{T}_{H_1}$  must be greater than  $\mathcal{T}$ ; otherwise, both  $Q_1$  and  $Z_1$  would have to be 1, which is impossible in practice. Thus, Algorithm 1 sets the initial search region for  $\mathcal{T}_{H_1}$  to  $(\mathcal{T}, 1)$ . The guessed value for  $\mathcal{T}_{H_1}$  in each iteration is at the center of this region, as expressed in line 6.

At each iteration, if the selected  $\mathcal{T}_{H_1}$  generates a configuration where the number of nodes is above  $N_{min}$ , it is assumed that  $Q_1$  can be enhanced by decreasing  $N$ , which allows for further decreasing  $\mathcal{T}_{H_1}$  in the next iteration. Conversely, if  $N < N_{min}$ ,  $\mathcal{T}_{H_1}$  is increased so that  $Q_1$  can be lower, allowing for more nodes in the network. This “binding” part of the algorithm is in lines 30-34.

Provided the branch-and-bound technique guesses  $\mathcal{T}_{H_1}$  in line 6, the range limits for all SF are computed using (18) in line 7. In the following, the algorithm uses the newly computed vector  $L$  to obtain vector  $B$  and matrix  $Y$  (lines 11-16), allowing for the computation of the PPPs densities in  $A$  (line 17), using (21). Following that, the number of nodes fitting the generated configuration is computed by first obtaining the area of each SF ring in lines 18-19 as  $V_i = \pi(l_i^2 - l_{i-1}^2)$ . The algorithm converges and stops when the difference in the radius  $R$  of the overall coverage area between two consecutive iterations is less than  $\chi$  (line 20) and  $N > N_{min}$  (line 21), where  $\chi$  defines the precision of  $R$ . If the variation of  $R$ , *i.e.*,  $\text{abs}(R - R_{last})$ , is too small and the algorithm did not achieve  $N_{min}$  yet, the algorithm keeps trying to converge until the variation in the guessed  $\mathcal{T}_{H_1}$  is below a threshold  $\epsilon$  (line 22), in which case the algorithm stops and announces a divergence. After evaluating the proposed algorithm for a set of test scenarios, we concluded that good values for the stopping thresholds are  $\chi = 1m$  and  $\epsilon = 10^{-9}$ .

Algorithm 1 always converges if there are feasible solutions to the problem. If the requirements of minimum network density ( $N_{min}$  and  $p$ ), targeted reliability ( $\mathcal{T}$ ), or both, are too high, however, the algorithm may take too long to converge. Hence, we stop the algorithm when the changes in  $\mathcal{T}_{H_1}$  get too small (line 22), thus guaranteeing that the algorithm will not run forever since  $\mathcal{T}_{H_1,max} - \mathcal{T}_{H_1,min}$  decreases every iteration. It is important to note, however, that achieving higher network density is always possible by reducing the reliability requirement  $\mathcal{T}$ . Moreover, highly demanding scenarios without feasible solutions or with lengthy convergence are not typical in LORAWAN, since the technology has been conceived to support massive rather than critical IoT applications.

The algorithm has linear complexity, *i.e.*,  $\mathcal{O}(n)$ . Analysis of convergence time of this method depends on the precision, which we define in Algorithm 1 as  $\chi = 1$  meter. Therefore, the literature defines the maximum number of iterations as  $n = \log_2 \left( \frac{\chi_0}{\chi} \right)$ , where  $\chi_0$  is the initial error [27]. In Algorithm 1,  $\chi_0 = |R_1 - R_0|$ , with  $R_0 = 0$  (Algorithm 1, line 3) and  $R_1$  computed in the first iteration (line 9) using (18) with  $\mathcal{T}_{H_1} = \frac{1+\mathcal{T}}{2}$  (line 6). Note that although Algorithm 1 involves the solution of a system of linear equations with matrix inversion (line 17) and matrix multiplications (line 19), these are computed quite efficiently since it handles low-dimension matrices – the largest matrix is  $\mathbf{Y}$ , which is 6-by-6.

### C. Maximization of Number of Nodes

Now we consider the case of maximizing the total number of nodes given restrictions of minimum coverage radius ( $R_{min}$ ) and average reliability ( $\mathcal{T}$ ). We use a more straightforward approach than in Algorithm 1. The problem of

maximizing the number of nodes is equivalent to the problem of minimizing  $Q_1$ . Thus it is straightforward to conclude, from (4), that we should maximize  $H_1$  because higher  $H_1$  allows for lower  $Q_1$ . Since we assume that the worst cases are at the edge of the SFs and we have a restriction on the coverage radius, the maximum possible  $H_1$  is that yielding  $l_6 = R_{min}$ . Thus, from (6), we conclude that  $\mathcal{T}_{H_1} = H_1(R_{min})$ . Assuming the same  $\mathcal{T}_{H_1}$  for all SFs, we use (18) to compute  $L$  and obtain the geometry of the network.

Once we obtain  $L$ , we get the maximum allowable densities ensuring  $\mathcal{T}$  through (21) as shown in Algorithm 2. Line 1 uses (6) to compute the maximum  $\mathcal{T}_{H_1}$  satisfying  $R_{min}$ . Line 2 uses the computed  $\mathcal{T}_{H_1}$  to obtain the geometry of the network  $L$ . The loop in lines 5-10 computes matrix  $Y$  and vector  $B$ , so the maximum device density vector  $A$  can be computed in line 11. Finally, after computing the areas of the rings and storing them in vector  $V$  (line 12), we obtain the maximum number of nodes in line 13.

---

**Algorithm 2** Maximization of the number of nodes given the target reliability ( $\mathcal{T}$ ) and the minimum coverage radius ( $R_{min}$ ).

---

**Input:**  $\mathcal{T}, p, R_{min}, \alpha_z$

**Output:** result,  $A, L, N_{max}$

```

1:  $\mathcal{T}_{H_1} \leftarrow \exp \left( -\frac{N\psi_6}{P_t g(R_{min})} \right)$ 
2:  $L \leftarrow \frac{\lambda}{4\pi} \left[ -\frac{P_t \ln(\mathcal{T}_{H_1})}{N\psi} \right]^{\frac{1}{\eta}}$  {Equation (1)}
3:  $R \leftarrow L[end]$ 
4:  $R_z \leftarrow R$ 
5: for  $i = [1, \dots, 6]$  do
6:   for  $j = [1, \dots, 6]$  do
7:      $Y[i, j] \leftarrow f(l_i, \delta_{i,j}, l_j, l_{j+1})$ 
8:   end for
9:    $B[i] \leftarrow -\frac{1}{2\pi} \ln \frac{\mathcal{T}}{Z_1(l_i)\mathcal{T}_{H_1}}$ 
10: end for
11:  $A \leftarrow Y^{-1} \times B$  {Equation (2)}
12:  $V \leftarrow \text{ComputeRingAreas}(L)$ 
13:  $N_{max} \leftarrow (Ap) \times V'$ 
14: if  $A_i \geq 0, \forall A_i$  then
15:   result  $\leftarrow 1$ 
16: else
17:   result  $\leftarrow -1$ 
18: end if
19: return result,  $A, L, N_{max}$ 

```

---

Note that Algorithm 2 is not iterative since there is no loop searching for the optimum solution and, therefore, it has complexity  $\mathcal{O}(1)$ . This algorithm merely describes how to use the proposed models to determine the optimum LORAWAN configuration considering the restrictions. The approach produces unfeasible configurations if the restrictions are too strict. Thus, lines 14-18 check whether the method generated non-negative densities for all SFs to assess whether the results are feasible or not.

## VI. NUMERICAL RESULTS

This section evaluates the proposed model and algorithms. In all figures, lines represent theoretical probabilities (*i.e.*,



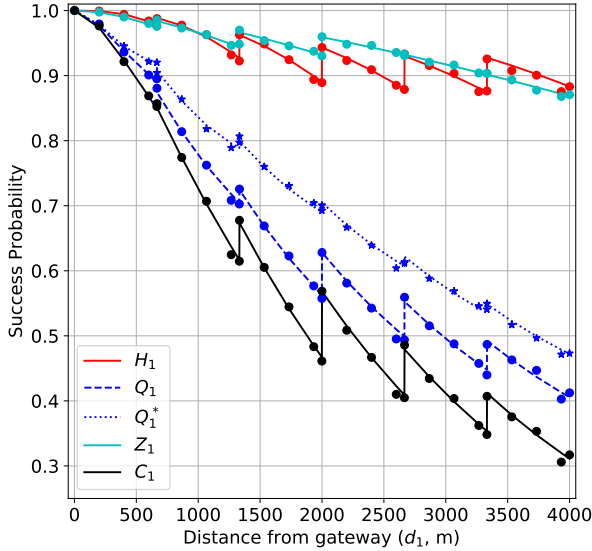


Figure 2. Success probabilities of all outage sources. LORA:  $\bar{N} = 4000$ ,  $p = 0.1\%$ ,  $\eta = 2.75$ ,  $\mathcal{P}_t = 14\text{dBm}$ ,  $R = 4000\text{m}$ . IEEE 802.15.4G:  $\bar{N}_z = 1000$ ,  $p_z = 0.1\%$ ,  $\eta = 2.75$ ,  $\mathcal{P}_t = 14\text{dBm}$ ,  $R_z = 4000\text{m}$ .

$H_1, Q_1, Z_1, Q_1^*$ ), while marks along the lines show the results of Monte Carlo simulations. Each mark in a figure is the average of  $10^5$  simulations considering random deployments. Moreover, we assume  $F = 6$  dB,  $\eta = 2.75$ ,  $\lambda = c/f$  m,  $c = 3 \times 10^8$  m/s (speed of light),  $f = 868$  MHz for both LORAWAN and IEEE 802.15.4G. LORAWAN channel bandwidth is  $B_l = 125$  kHz, and IEEE 802.15.4G channel bandwidth is  $B_z = 200$  kHz. We also assume that nodes in LORAWAN and IEEE 802.15.4G transmit with  $\mathcal{P}_t = 14\text{dBm}$ . These parameters configure typical European suburban scenarios.

Concerning IEEE 802.15.4G interference, we evaluate the algorithms considering three scenarios. In real deployments, the designer of a LORAWAN network may not know the operational parameters of the interfering IEEE 802.15.4G network. Thus, in a practical situation, the designer should assume worst-case configurations for the external network.

#### A. Model Validation

Figure 2 aims to validate the presented models by showing the success rates  $H_1, Q_1, Z_1$ , and  $C_1$  as a function of the distance from the gateway. The scenario considers an average number of nodes  $\bar{N} = 4000$ , transmitting with duty cycle  $p = 0.1\%$  in a circular area around the gateway with radius  $R = 4000\text{m}$ . The IEEE 802.15.4G network generating external interference has  $\bar{N}_z = 1000$  nodes transmitting with duty cycle  $p_z = 0.1\%$ , also in a circular area with radius  $R_z = 4000\text{m}$ . As can be seen, all theoretical expressions (lines) match the simulation results (marks). One can observe in  $Z_1$  that a relatively light interference from IEEE 802.15.4G ( $\bar{N}_z = 1000, p_z = 0.1\%$ ) has little impact in lower SFs due to the smaller ToA and reduced probability of concurrent transmissions. Higher SFs, on the other hand, have higher ToA and thus suffer more from this external interference.

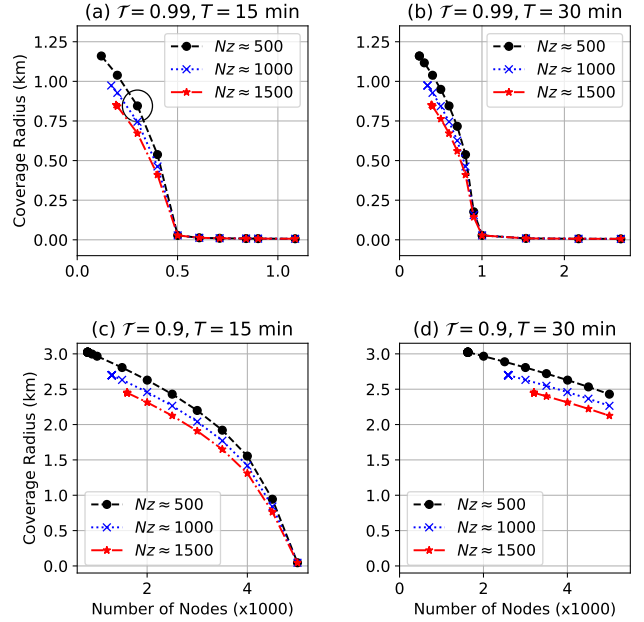


Figure 3. Optimization between coverage and number of nodes given a minimum reliability constraint when maximizing  $R$  with Algorithm 1.

Also, in Figure 2,  $Q_1^*$  shows what the capture probability would be if we consider that LORA signals are perfectly orthogonal. We obtain  $Q_1^*$  from (14) by considering only  $j = i$ . As can be seen, the gap between  $Q_1$  and  $Q_1^*$  shows that inter-SF interference plays a vital role in link quality.

#### B. Algorithm 1: Maximization of Range

Now we evaluate Algorithm 1 of Section V-B. These results use the same network parameters employed to validate the network model. Figure 3 presents a series of graphs for varying optimization objectives. Plots in the same row consider the same reliability target  $\mathcal{T}$ , while plots in the same column use the same packet generation interval  $T$ , expressed in minutes. Each graph shows three curves, each one considering a different amount of IEEE 802.15.4G interference, which varies by changing the number of IEEE 802.15.4G nodes ( $\bar{N}_z$ ), always with duty cycle  $p_z = 0.1\%$ . Each optimization point considers different  $N_{min}$  values, evaluated every 100m.

The first conclusion, when comparing the curves in all plots, is that different IEEE 802.15.4G interference leads to shorter communication ranges when following our proposed optimization procedure. That makes sense since shorter distances feature smaller path loss, making signals less susceptible to external interference. It is also possible to observe that less stringent reliability targets lead to larger coverage areas. Again, that makes sense since smaller  $\mathcal{T}$  yields smaller  $\mathcal{T}_{H_1}$ , which in turn enables longer communication range.

Also, in Figure 3, plot (a) shows the more rigorous scenario; the configuration allowing the required reliability is only practical for  $N_{min} \leq 400$  nodes, with a radius varying from 410 to 1160 meters, depending on  $N_{min}$  and the external interference. The coverage radius with  $N_{min} \geq 500$  either converged to unpractical distances of less than 10 meters or diverged,



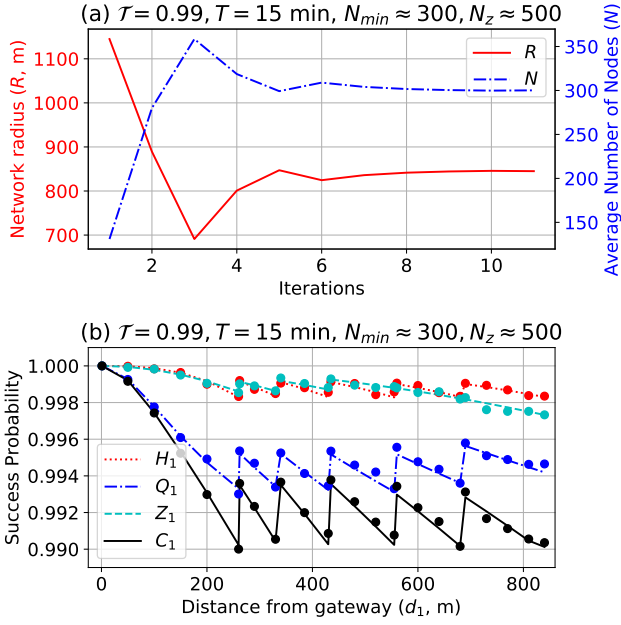


Figure 4. Convergence of Algorithm 1 and success probability for the scenario marked in Figure 3a.

meaning that we could not place this many LORAWAN nodes with packet generation interval of 15 minutes while ensuring minimum reliability of  $\mathcal{T} = 0.99$ .

For  $\mathcal{T} = 0.99$ , there are more feasible scenarios if network usage decreases. Plot 3b shows that configurations with up to 900 nodes are possible if the packet transmission interval is  $T = 30$  minutes. For  $\mathcal{T} = 0.9$  with  $T = 15$  minutes, it is possible to find reasonably good network configurations up to  $N_{min} = 4500$ . However,  $N_{min} = 5000$  shrinks the communication range to unpractical distances.

Figure 4 illustrates the behavior of Algorithm 1 and network performance when taking the circled case in Figure 3a as an example. Figure 4a shows the convergence of  $R$  and  $\bar{N}$  for this scenario. Applying the estimate of the number of iterations presented in Section V-B to this example makes  $R_1 = 1244.7\text{m}$  because of  $\mathcal{T} = 0.99$ . Therefore, the maximum number of iterations to reach  $|R - R_{last}| < \chi$  (line 20, Algorithm 1) is  $n = \log_2\left(\frac{\chi_0}{\chi}\right) = \log_2\left(\frac{1244.7}{1}\right) = 10.28$ . We see in Figure 4a that the algorithm converges after the 11th iteration with  $\bar{N} = 300.1$ , thus “stretching” the network range as much as possible. Also, note that convergence time depends on  $\chi_0$ , which in turn depends on  $\mathcal{T}$ . If we consider the same case above with  $\mathcal{T} = 0.9$  or  $\mathcal{T} = 0.8$ , we would have, respectively,  $\chi_0 = 2899.7$  or  $\chi_0 = 3767.3$ , what would make, respectively,  $n = 11.50$  or  $n = 11.88$ , showing that the impact of  $\mathcal{T}$  in convergence time is small.

Table II shows numerical results of the same scenario in two columns: “All sources” with the results for our complete model; and “Intra-SF only” disregarding both inter-SF and external interference sources. We get the results in the “Intra-SF only” column using the same models, but setting  $\theta_i = -\infty, \forall i \in S$  in  $\Theta$ , and  $\delta_{i,j} = 1$  for  $i = j$  and  $\delta_{i,j} = -\infty$  otherwise. When considering all sources of interference, as

Table II  
DETAILED OPTIMIZATION RESULTS FOR THE MARKED SCENARIO IN FIGURE 3A.

Interference:		All sources			Intra-SF only		
Scenario	SF	Range (m)	$\bar{N}_i$	$\bar{N}$	Range (m)	$\bar{N}_i$	$\bar{N}$
3a	7	261.6	162.8	300.1	370.0	124.6	300.0
	8	336.4	67.5		475.7	87.1	
	9	432.4	32.5		611.6	43.5	
	10	555.9	21.8		786.2	25.3	
	11	685.4	10.6		969.3	12.9	
	12	845.0	4.7	1195.1	6.4		

expected, the fact that ToA impacts the duty cycle induces the optimization procedure to allocate most of the nodes with lower SF. That happens because signal attenuation increases with distance, making more distant nodes more vulnerable to both internal and external interference. Recall that a shorter ToA reduces the collision probability. Moreover, longer ToA generates more internal interference to other SFs.

In some cases, higher SFs may not be used to ensure minimum reliability. However, note that (18), (21), and Algorithm 1 can be extended to change the restriction  $N_{min}$  to represent a vector with the minimum number of nodes using each SF. One can achieve that by revisiting the computation of the densities in (21) to consider such a minimum number of nodes when computing the spatial density. Since doing that will possibly result in more nodes using higher SFs, it is expected that fewer nodes use lower SF, resulting in a smaller total number of nodes, as well as a shorter network radius, since the algorithm will converge to a higher  $H_1$  to compensate the increased  $Q_1$ . When disregarding inter-SF and external interference, we observe that higher SFs are profoundly affected by inter-SF and external interference, mainly due to their extended ToA. In particular, we observe that interference, rather than path loss, is the main factor for which our method disfavors the use of higher SF. Moreover, it is clear that interference considerably affects coverage.

Finally, Figure 4b shows the success probabilities of the example scenario, where the optimized configurations consider the minimum average reliability target  $\mathcal{T}$  for all distances from the gateway. As expected, the success probability approaches the desired minimum  $\mathcal{T} = 0.99$  at the edge of each SF. We can see that collisions ( $Q_1$ ) are kept almost constant or increase slightly with SF. That happens because the algorithm reduces the number of nodes using each SF to keep  $Q_1$  in pace with  $H_1$  and  $Z_1$ , to ensure the minimum  $\mathcal{T}$ .

### C. Algorithm 2: Maximization of Nodes

Now we evaluate Algorithm 2 of Section V-C. The plots in Figure 5 show the results for different scenarios of required minimum reliability ( $\mathcal{T}$ ) and message generation period ( $T$ ). For all plots, the x-axis represents the  $R_{min}$  input to the algorithm, while the y-axis shows the achieved maximized number of nodes. In each plot, the x-axis grows up to the value for which the requirements yield practical results.

In Figure 5, if we analyze each row of plots independently, we see that the maximum number of nodes is a linear func-

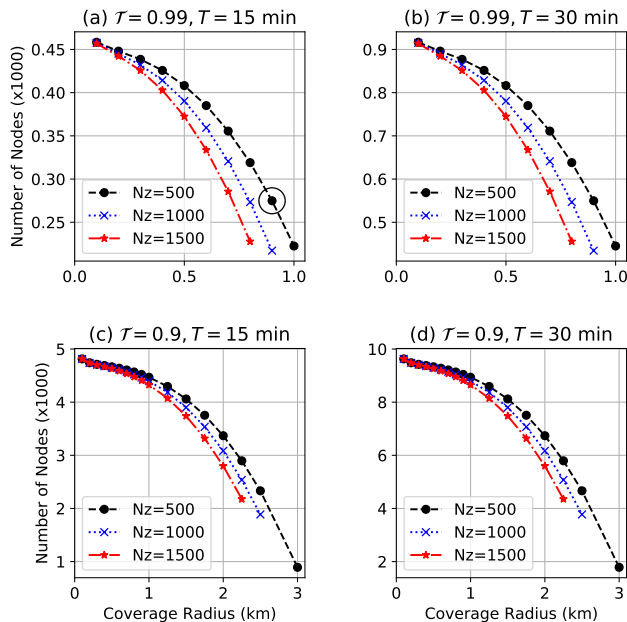


Figure 5. Optimization between the number of nodes and coverage given a minimum reliability constraint when maximizing  $\bar{N}$  with Algorithm 2.

Table III  
DETAILED OPTIMIZATION RESULTS FOR THE MARKED SCENARIO IN FIGURE 5A.

Interference:		All sources			Intra-SF only		
Scenario	SF	Range (m)	$\bar{N}_i$	$\bar{N}$	Range (m)	$\bar{N}_i$	$\bar{N}$
5a	7	278.7	149.2	274.9	278.7	211.1	508.2
	8	358.3	61.8		358.3	147.6	
	9	460.6	29.9		460.6	73.7	
	10	592.1	20.2		592.1	42.9	
	11	730.0	9.5		730.0	21.8	
	12	900.0	4.0		900.0	10.9	

tion of the transmission period  $T$ . For instance, considering  $R_{min} = 500\text{m}$  and  $N_z = 500$ ,  $N_{max}$  in plots 5a and 5b are, respectively, 408.18 and 816.36, *i.e.*,  $N_{max}$  doubles when  $T$  doubles. That is expected since these variations ensure the same network load in all scenarios. We also observe, in all plots, that increased external interference reduces both the number of nodes and the achievable coverage radius.

Table III shows the achieved geometry and number of nodes of the marked scenario of Figure 5a. Again, the ‘‘All sources’’ column presents the results of our complete model, while the ‘‘Intra-SF only’’ column disregards inter-SF and external interference. Since the method assumes that the maximum number of nodes is achieved with the shortest possible distances, the maximum range of a node using SF<sub>12</sub> has to be  $R_{min}$  (900m for this case). As for Algorithm 1, Algorithm 2 also favors lower SFs. Moreover, Table III shows that the maximum number of nodes almost doubles when disregarding inter-SF and external interference, emphasizing the importance of taking such impairments into account to avoid overestimating the network performance. Finally, Figure 6 shows success probabilities for the example scenario, which approach

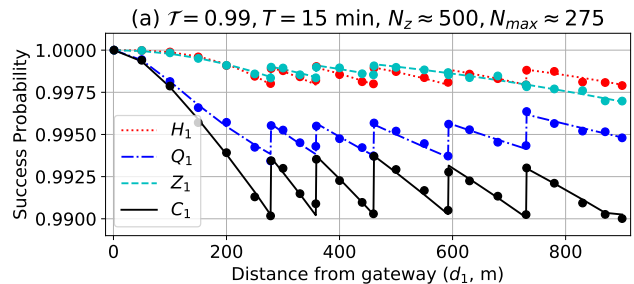


Figure 6. Average outage expectation for the marked scenario in Figure 5a.

$\mathcal{T} = 0.99$  at SF edges but stay above the required minimum  $\mathcal{T}$  for all distances shorter than  $R_{min}$ .

## VII. CONCLUSION

This paper presents two algorithms to optimize the configuration of LORAWAN under imperfect SF orthogonality and IEEE 802.15.4G interference. We use models of LORAWAN networks to derive success probabilities of packet delivery under internal and external (IEEE 802.15.4G) interference. The presented algorithms search for optimum LORAWAN configurations given restrictions of minimum network density or coverage radius, meeting a target minimum reliability level. The analytic results are validated using simulations.

Regarding IEEE 802.15.4G interference over LORAWAN, although higher SF should be more robust to this type of interference, they suffer more from that impairment because their increased ToA makes it more likely that transmissions overlap with IEEE 802.15.4G activity. Finally, regarding the proposed algorithms, they provide a tool for exploring trade-offs between network load and coverage range by showing the feasible region of LORAWAN network configurations.

Possible future extensions of this work can include other important LPWAN features, such as power allocation and multiple base stations. Moreover, one may consider adapting the proposed algorithms to maximize reliability given fixed network geometry and number of users, in a way similar to what [28] does, or to analyze latency and energy efficiency of the models, similarly to [29], noting that neither [28] nor [29] consider LORAWAN networks. In the future, we also plan to validate our models using data from a multi-technology large scale IoT network at the University of Oulu.

### APPENDIX A: SOLUTION OF $f(d_1, \gamma, l_a, l_b)$

Here we solve the integral in (10). Let

$$f(d_1, \gamma, l_a, l_b) = \int_{l_a}^{l_b} \frac{\gamma d_1^\eta}{x^\eta + \gamma d_1^\eta} x \, dx.$$

We rearrange  $f(\cdot)$  as

$$f(d_1, \gamma, l_a, l_b) = \int_{l_a}^{l_b} x \left( \frac{x^\eta}{d_1^\eta \gamma} + 1 \right)^{-1} dx$$

and use the binomial theorem  $(x+1)^{-1} = \sum_{k=0}^{\infty} (-1)^k x^k$  to obtain

$$f(d_1, \gamma, l_a, l_b) = \int_{l_a}^{l_b} \sum_{k=0}^{\infty} \left( \frac{-1}{d_1^\eta \gamma} \right)^k x^{\eta k + 1} dx.$$

Since  $f(\cdot)$  is continuous in  $\mathbb{R} \forall x > 0$ , we interchange the sum and the integration and solve the integral, yielding

$$f(d_1, \gamma, l_a, l_b) = \sum_{k=0}^{\infty} \left( \frac{-1}{d_1^\eta \gamma} \right)^k \frac{x^{2+\eta k}}{\eta k + 2} \Bigg|_{l_a}^{l_b}.$$

We resort to the Pochhammer function  $(a)_k = a(a+1) \cdots (a+k-1) = \frac{\Gamma(a+k)}{\Gamma(a)}$  and to  $\frac{(b)_k}{(b+1)_k} = \frac{b}{b+k}$ , and reorganize  $f(\cdot)$  as

$$f(d_1, \gamma, l_a, l_b) = \frac{x^2}{2} \sum_{k=0}^{\infty} \frac{(1)_k}{k!} \frac{\left(\frac{2}{\eta}\right)_k}{\left(1 + \frac{2}{\eta}\right)_k} \left(-\frac{x^\eta}{d_1^\eta \gamma}\right)^k \Bigg|_{l_a}^{l_b},$$

which is in the form of the Gaussian Hypergeometric function  ${}_2F_1(a, b; c; z) = \sum_{k=0}^{\infty} \frac{(a)_k (b)_k z^k}{(c)_k k!}$  [30], what yields

$$f(d_1, \gamma, l_a, l_b) = \frac{x^2}{2} {}_2F_1\left(1, \frac{2}{\eta}; 1 + \frac{2}{\eta}; -\frac{x^\eta}{d_1^\eta \gamma}\right) \Bigg|_{l_a}^{l_b}.$$

## REFERENCES

- [1] M. Centenaro, L. Vangelista, A. Zanella, and M. Zorzi, "Long-range communication in unlicensed bands: the rising stars in the IoT and smart city scenarios," *IEEE Wireless Communications*, vol. 23, no. 5, pp. 60–67, Oct 2016.
- [2] C. Bockelmann, N. Pratas, H. Nikopour, K. Au, T. Svensson, C. Stefanovic, P. Popovski, and A. Dekorsy, "Massive machine-type communications in 5G: physical and MAC-layer solutions," *IEEE Communications Magazine*, vol. 54, no. 9, pp. 59–65, Sep 2016.
- [3] LoRa Alliance. (2019, Sep) Website. [Online]. Available: <http://www.lora-alliance.org>
- [4] Wi-SUN Alliance. (2019, Sep) Website. [Online]. Available: <http://www.wi-sun.org>
- [5] K.-H. Chang and R. Mason, "The IEEE 802.15.4g standard for smart metering utility networks," in *IEEE 3rd International Conference on Smart Grid Communications*, Nov 2012, pp. 476–480.
- [6] L. Zhang, Y. Liang, and M. Xiao, "Spectrum sharing for internet-of-things: A survey," *IEEE Wireless Communications*, vol. 26, no. 3, pp. 132–139, Jun 2019.
- [7] C. Orfanidis, L. M. Feeney, M. Jacobsson, and P. Gunningberg, "Investigating interference between LoRa and IEEE 802.15.4g networks," in *IEEE 13th International Conference on Wireless and Mobile Computing, Networks and Communications*, Oct 2017, pp. 1–8.
- [8] L. Krupka, L. Vojtech, and M. Neruda, "The issue of LPWAN technology coexistence in IoT environment," in *17th International Conference on Mechatronics (Mechatronika)*, Dec 2016.
- [9] E. D. Poorter, J. Hoebeke, M. Strobbe, I. Moerman, S. Latré, M. Weyn, B. Lannoo, and J. Famaey, "Sub-GHz LPWAN network coexistence, management and virtualization: An overview and open research challenges," *Wireless Personal Communications*, vol. 95, no. 1, pp. 187–213, Jul 2017.
- [10] A. Hoeller-Jr, R. D. Souza, O. L. A. López, H. Alves, M. de Noronha-Neto, and G. Brante, "Analysis and performance optimization of LoRa networks with time and antenna diversity," *IEEE Access*, vol. 6, pp. 32 820–32 829, Jul 2018.
- [11] A. Mahmood, E. G. Sisinni, L. Guntupalli, R. Rondón, S. A. Hassan, and M. Gidlund, "Scalability analysis of a LoRa networks under imperfect orthogonality," *IEEE Transactions on Industrial Informatics*, vol. 15, no. 3, pp. 1425–1436, Mar 2019.
- [12] R. B. Sørensen, D. M. Kim, J. J. Nielsen, and P. Popovski, "Analysis of latency and MAC-layer performance for Class A LoRaWAN," *IEEE Wireless Communications Letters*, vol. 6, no. 5, pp. 566–569, Oct 2017.
- [13] O. Georgiou and U. Raza, "Low power wide area networks analysis: Can LoRa scale?" *IEEE Wireless Communications Letters*, vol. 6, no. 2, pp. 162–165, Apr 2017.
- [14] N. Abramson, "The ALOHA system – another alternative for computer communications," in *Fall Joint Computer Conference*, Dec 1970, pp. 281–285.
- [15] ANI20.22 LoRa Modulation Basics, Semtech Corporation, Mar 2015.
- [16] SX1272/73 - 860 MHz to 1020 MHz Low Power Long Range Transceiver, Semtech Corporation, Mar 2017.
- [17] D. Croce, M. Gucciardo, S. Mangione, G. Santaromita, and I. Tinnirello, "Impact of LoRa imperfect orthogonality: Analysis of link-level performance," *IEEE Communications Letters*, vol. 22, no. 4, pp. 796–799, Apr 2018.
- [18] IEEE Std 802.15.4g-2012, "IEEE standard for local and metropolitan area networks - Part 15.4: Low-rate wireless personal area networks (LR-WPANs) amendment 3: Physical layer (PHY) specifications for low-data-rate, wireless, smart metering utility networks," Apr 2012.
- [19] M. K. Oh, J. Y. Kim, S. Lee, Y. Jeon, and S. Choi, "A fully integrated IEEE 802.15.4g MR-FSK SoC for smart utility network applications," *IEEE Transactions on Consumer Electronics*, vol. 60, no. 4, pp. 580–586, Nov 2014.
- [20] H. Harada, K. Mizutani, J. Fujiwara, K. Mochizuki, K. Obata, and R. Okumura, "IEEE 802.15.4g Based Wi-SUN Communication Systems," *IEICE Transactions on Communications*, vol. E100.B, no. 7, pp. 1032–1043, 2017.
- [21] J. Muñoz, T. Chang, X. Vilajosana, and T. Watteyne, "Evaluation of IEEE 802.15.4g for environmental observations," *Sensors (Basel)*, vol. 18, no. 10, 2018.
- [22] IEEE Std 802.15.4e-2012, "IEEE standard for local and metropolitan area networks - part 15.4: Low-rate wireless personal area networks (LR-WPANs) amendment 1: MAC sublayer," Apr 2012.
- [23] U. Deshpande, D. Kotz, and C. McDonald, "Coordinated sampling to improve the efficiency of wireless network monitoring," in *15th IEEE International Conference on Networks*, Nov 2007, pp. 353–358.
- [24] M. Haenggi, *Stochastic Geometry for Wireless Networks*. USA: Cambridge University Press, 2012.
- [25] A. Goldsmith, *Wireless Communications*. USA: Cambridge University Press, 2005.
- [26] C. Goursaud and J.-M. Gorce, "Dedicated networks for IoT: PHY/MAC state of the art and challenges," *EAI Endorsed Transactions Internet-of-Things*, vol. 15, no. 1, pp. 1–11, Oct 2015.
- [27] R. L. Burden, D. J. Faires, and A. M. Burden, *Numerical Analysis*. USA: Cengage Learning, 2016.
- [28] J. Jia, Y. Deng, J. Chen, A. H. Aghvami, and A. Nallanathan, "Achieving high availability in heterogeneous cellular networks via spectrum aggregation," *IEEE Transactions on Vehicular Technology*, vol. 66, no. 11, pp. 10 156–10 169, Nov 2017.
- [29] A. Mukherjee, "Energy efficiency and delay in 5G ultra-reliable low-latency communications system architectures," *IEEE Network*, vol. 32, no. 2, pp. 55–61, March 2018.
- [30] A. B. O. Daalhuis, "Hypergeometric function," in *NIST Handbook of Mathematical Functions*, 1st ed., F. W. J. Olver, D. W. Lozier, R. F. Boisvert, and C. W. Clark, Eds. New York, USA: Cambridge University Press, 2010, ch. 15, pp. 383–402.